A New Geostatistical Solution to Remote Sensing Image Downscaling

Qunming Wang, *Member, IEEE*, Wenzhong Shi, Peter M. Atkinson, and Eulogio Pardo-Igúzquiza

Abstract—The availability of the panchromatic (PAN) band in remote sensing images gives birth to so-called image fusion techniques for increasing the spatial resolution of images to that of the PAN band. The spatial resolution of such spatially sharpened images, such as for the MODIS and Landsat sensors, however, may not be sufficient to provide the required detailed land-cover/land-use information. This paper proposes an area-to-point regression kriging (ATPRK)-based geostatistical solution to increase the spatial resolution of remote sensing images beyond that of any input images, including the PAN band. The new approach is a two-stage approach, including covariate downscaling and ATPRK-based image fusion. The new approach treats the PAN band as the covariate and takes advantages of its textural information. It explicitly accounts for the size of support, spatial correlation, and the point spread function of the sensor and has the characteristic of perfect coherence with the original coarse data. Moreover, the new downscaling approach can be extended readily by incorporating other ancillary information. The proposed approach was examined using both Landsat and MODIS images. The results show that it can produce more accurate sharpened images than four benchmark approaches.

Index Terms—Area-to-point regression kriging (ATPRK), downscaling, geostatistics, image fusion, Landsat Enhanced Thematic Mapper, Moderate Resolution Imaging Spectroradiometer (MODIS).

I. INTRODUCTION

THE Moderate Resolution Imaging Spectroradiometer (MODIS) and Landsat sensors can revisit the Earth regularly. Their products (i.e., MODIS and Landsat images) are freely available, and the swath is much wider than the commercial high-resolution images such as QuickBird, WorldView, and IKONOS. These advantages lead to the popular use of MODIS and Landsat images in global land-cover/land-use (LCLU) monitoring, such as the use of 500-m MODIS data (i.e., bands 1–7) in detecting deforestation processes [1] and 30-m Landsat data in detecting urbanization processes [2]. However, they provide coarse spatial resolutions relative to the requirements of some applications within these domains. For example, deforestation generally occurs at a spatial resolution finer than the 500-m pixel size of MODIS, and changes in small residential buildings are usually at a resolution finer than the 30-m pixel size of Landsat.

There is a great need for downscaling techniques that can increase the spatial resolution of such data. MODIS bands 1 and 2 have a 250-m spatial resolution, whereas Landsat Enhanced Thematic Mapper Plus (ETM+) images contain a 15-m panchromatic (PAN) band. The fine spatial, but coarse spectral, resolution bands can be combined with coarse spatial, but fine spectral, resolution bands to generate a fine spatial and spectral resolution image, using image fusion techniques such as pansharpening. A variety of image fusion algorithms have been developed over the past decades, including the intensity–hue–saturation [3], Brovey [4], principal component analysis [5], wavelet transformation [6], [7], high-pass filter (HPF) [3], [7], and spare representation [8] methods, as well as the automated statistics-based fusion method implemented in PCI Geomatica [9]. It is beyond the scope of this paper to explicitly review existing image fusion methods, but several reviews on such approaches exist [10]–[14].

Recently, the application of geostatistical solutions for image fusion-based downscaling has increased, based on their significant advantage in preserving the spectral properties of the observed coarse images. Pardo-Iguzquiza *et al.* [15] sharpened Landsat images using a one-stage downscaling cokriging (DSCK) method, in which each observed coarse band was considered as the primary variable and the fine PAN band was considered as the secondary variable. In their later work, DSCK was extended with a spatially adaptive filtering scheme [16]. In view of the complex cross-semivariogram modeling, Sales *et al.* [17] proposed a kriging with external drift (KED) approach to downscale MODIS images, which requires only autosemivariogram modeling and is easier to implement than DSCK. KED, however, suffers from expensive computational cost, as it needs to compute kriging weights locally for each fine pixel [17]. Wang *et al.* [18] first introduced the area-to-point regression kriging (ATPRK) concept in a remote sensing context and proposed it for MODIS image downscaling. ATPRK is fast, user friendly, and can readily incorporate fine spatial resolution information provided by other supplementary data.

Q. Wang is with the Department of Land Surveying and Geo-Informatics, The Hong Kong Polytechnic University, Kowloon, Hong Kong (e-mail: wqm11111@126.com).

W. Shi is with The Hong Kong Polytechnic University, Kowloon, Hong Kong, and also with Wuhan University, Wuhan 430072, China (e-mail: lswzshi@polyu.edu.hk).

P. M. Atkinson is with the Faculty of Science and Technology, Lancaster University, Lancaster LA1 4YR, U.K., with the Faculty of Geosciences, University of Utrecht, 3584 CS Utrecht, The Netherlands, with the School of Geography, Archaeology and Palaeoecology, Queen's University Belfast, Belfast BT7 1NN, U.K., and also with Geography and Environment, University of Southampton, Southampton SO17 1BJ, U.K. (e-mail: P.M.Atkinson@lancaster.ac.uk).

E. Pardo-Igúzquiza is with Instituto Geológico y Minero de España, 28003 Madrid, Spain (e-mail: e.pardo@igme.es).

The aforementioned image fusion approaches, including the geostatistical solutions, were generally designed to downscale coarse images to the spatial resolution of the PAN or PAN-like (i.e., band 1 or 2 in MODIS data; hereafter also PAN for simplicity) bands. However, in many cases, the 250-m fused MODIS and 15-m Landsat product may not be sufficient to provide detailed LCLU information, as the size of the objects of interest in MODIS or Landsat images may be smaller than 250- or 15-m. In this case, it is necessary to develop downscaling approaches that can predict pixel values at a spatial resolution finer than that of all available images, including the PAN band, to provide more LCLU information.

Atkinson *et al.* [19] extended the DSCK approach to cases where the pixel size to be predicted is smaller than that of all input variables. The applicability of the extended DSCK approach was demonstrated using a Landsat ETM+ data set. As aforementioned, however, DSCK requires complex semivariogram modeling, which makes it difficult to automate [17].

In pansharpening, it is of great interest to downscale the images to spatial resolutions finer than that of PAN, which is particularly significant for MODIS and Landsat data interpretation. For clarity, hereafter, the observed bands to be fused, the PAN, and the target bands to be predicted are called the coarse, intermediate, and fine bands, respectively, according to their relative spatial resolutions. In this paper, as an alternative to DSCK, ATPRK is extended to the case where the intermediate PAN band is available as the covariate. It is an extension of the original ATPRK approach developed in [18], where the target variables are of the same spatial resolution as the PAN band. Alternatively, the ATPRK-based downscaling approach in this paper involves two stages. The covariates (e.g., the PAN image) are first downscaled to the target fine spatial resolution, and then, the derived fine PAN image is used for ATPRK-based sharpening.

ATPRK is a new image fusion approach, which consists of regression modeling and area-to-point kriging (ATPK)-based residual downscaling [18]. It treats the PAN band as the covariate and models the overall trend in the target variables (i.e., fine pixels to be predicted) by regression. ATPRK is not only a newly developed regression kriging approach [20], [21] with ATPK for kriging interpolation but also an enhanced ATPK approach [22], [23] that incorporates fine spatial resolution ancillary data (e.g., the PAN band in pansharpening) through regression modeling. The ATPRK-based downscaling approach proposed in this paper has the following properties and advantages.

1) The use of intermediate spatial resolution covariates (e.g., the PAN image) can enhance the quality of fused images.
2) ATPRK accounts for the size of support, spatial correlation, and the point spread function (PSF) of the sensor.
3) ATPRK can perfectly preserve the spectral properties, that is, when upscaling the fused image to the original coarse spatial resolution, it is identical to the original one across all bands.
4) Different from DSCK in [19], ATPRK does not involve cross-semivariogram modeling, and the sizes of matrices in the kriging system are much smaller and, thus, more user friendly.
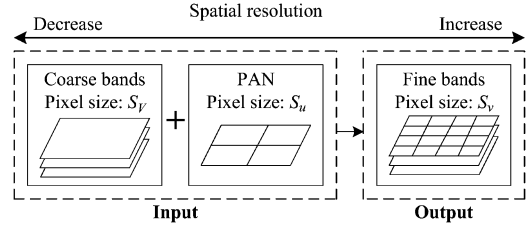

Fig. 1. Downscaling problem.

5) Other supplementary data at any spatial resolution finer than the primary variables (i.e., the coarse image to be downscaled) can be readily incorporated for possible enhancement.

The remainder of this paper is organized as follows. Section II introduces the principles of the proposed ATPRK in detail. In Section III, experimental results for the MODIS and Landsat data sets are provided to demonstrate the applicability of the new approach. Section IV further discusses the proposed approach, followed by a conclusion in Section V.

II. METHODS

A. Downscaling Problem

Let $Z_V^l(\mathbf{x}_i)$ be the random variable of pixel V centered at $\mathbf{x}_i$ ($i = 1, \ldots, M$, where M is the number of pixels) in coarse band l and $Z_u(\mathbf{x}_j)$ be the random variable of pixel u centered at $\mathbf{x}_j$ ($j = 1, \ldots, MF^2$, where F is the spatial resolution (zoom) ratio between the coarse and PAN bands) in the PAN band. The notations u and V denote the intermediate and coarse pixels, respectively. The objective of downscaling in this paper is to predict target variable $\hat{Z}_v^l(\mathbf{x})$ ($S_v < S_u < S_V$, where S_v, S_u, and S_V are the sizes of pixels v, u, and V, respectively) for all fine pixels in all coarse bands. Fig. 1 sketches the downscaling problem.

B. Downscaling Covariates in ATPRK

In ATPRK, the covariates are used for overall trend prediction of $\hat{Z}_v^l(\mathbf{x})$ and play an important role in the downscaling process, as they provide valuable finer spatial resolution texture information than the observed coarse data. The covariates need to be at the same spatial resolution as the target variables. In this paper, the covariates are proposed to be downscaled to the target fine spatial resolution using general ATPK. For the MODIS and Landsat images, this means using ATPK to downscale the intermediate PAN band Z_u to fine PAN band $\hat{Z}_v$. In the MODIS images, there are two intermediate bands (bands 1 and 2). For each coarse band, we select one band as PAN by measuring the spectral similarity [in terms of correlation coefficient (CC)] between it and the two intermediate bands, and the intermediate band with greater CC is selected as PAN.

ATPK refers to prediction on a support that is smaller than that of the original data [24]. It is distinguished from conventional centroid-based kriging, which ignores the spatial support and treats it always as equivalent to the observation support. ATPK explicitly accounts for the size of support, spatial correlation, and the PSF of the sensor. It predicts variables

from areal supports to points (i.e., pixels at the target fine spatial resolution in this paper) using semivariogram deconvolution to parameterize the random function model and kriging for prediction. Moreover, another appealing advantage associated with ATPK is its coherence property [22], [23], that is, the original coarse data can be perfectly preserved in predictions. The advantages encourage its development in downscaling.

Based on ATPK, the prediction for fine pixel v centered at a specific location $\mathbf{x}_0$ in the PAN band (i.e., $\hat{Z}_v(\mathbf{x}_0)$) is a linear combination of N intermediate observations in Z_u, i.e.,

$$\hat{Z}_v(\mathbf{x}_0) = \sum_{i=1}^{N_1} \lambda_i Z_u(\mathbf{x}_i), \quad \text{s.t.} \sum_{i=1}^{N_1} \lambda_i = 1 \tag{1}$$

in which λ_i is the weight for the ith intermediate pixel centered at $\mathbf{x}_i$. The N_1 pixels surround the pixel centered at $\mathbf{x}_0$, such as the $N_1 = 5 \times 5$ window of pixels. Thus, the spatial correlation between coarse pixels is accounted for in ATPK.

The task becomes the estimation of weights $\{\lambda_1, \ldots, \lambda_{N_1}\}$ in (1). They are calculated by minimizing the prediction error variance, and the corresponding kriging system is

$$\begin{bmatrix} \gamma_{uu}(\mathbf{x}_1, \mathbf{x}_1) & \cdots & \gamma_{uu}(\mathbf{x}_1, \mathbf{x}_{N_1}) & 1 \\ \vdots & \ddots & \vdots & \vdots \\ \gamma_{uu}(\mathbf{x}_{N_1}, \mathbf{x}_1) & \cdots & \gamma_{uu}(\mathbf{x}_{N_1}, \mathbf{x}_{N_1}) & 1 \\ 1 & \cdots & 1 & 0 \end{bmatrix} \begin{bmatrix} \lambda_1 \\ \vdots \\ \lambda_{N_1} \\ \theta \end{bmatrix}$$
$$= \begin{bmatrix} \gamma_{vu}(\mathbf{x}_0, \mathbf{x}_1) \\ \vdots \\ \gamma_{vu}(\mathbf{x}_0, \mathbf{x}_{N_1}) \\ 1 \end{bmatrix}. \tag{2}$$

In (2), $\gamma_{uu}(\mathbf{x}_i, \mathbf{x}_j)$ is the intermediate-to-intermediate semivariogram between intermediate pixels centered at $\mathbf{x}_i$ and $\mathbf{x}_j$, $\gamma_{vu}(\mathbf{x}, \mathbf{x}_j)$ is the fine-to-intermediate semivariogram between fine and intermediate pixels centered at $\mathbf{x}_0$ and $\mathbf{x}_j$, and θ is the Lagrange multiplier.

Let $\mathbf{s}$ be the Euclidean distance between the centroids of any two pixels, $\gamma_{vv}(\mathbf{s})$ be the fine-to-fine semivariogram between two fine pixels, and $h_u(\mathbf{s})$ be the PSF. The fine-to-intermediate semivariogram $\gamma_{vu}(\mathbf{s})$ and the intermediate-to-intermediate semivariogram $\gamma_{uu}(\mathbf{s})$ in (2) are calculated by convoluting $\gamma_{vv}(\mathbf{s})$ with the PSF, i.e.,

$$\gamma_{vu}(\mathbf{s}) = \gamma_{vv}(\mathbf{s})^* h_u(\mathbf{s}) \tag{3}$$

$$\gamma_{uu}(\mathbf{s}) = \gamma_{vv}(\mathbf{s})^* h_u(\mathbf{s})^* h_u(-\mathbf{s}) \tag{4}$$

in which $*$ is the convolution operator.

Based on the assumption that the pixel value is the average of the fine pixel values within it, the PSF is

$$h_u(\mathbf{x}) = \begin{cases} \frac{1}{S_u}, & \text{if } \mathbf{x} \in u(\mathbf{x}) \\ 0, & \text{otherwise} \end{cases} \tag{5}$$

where $u(\mathbf{x})$ is the spatial support of pixel u centered at $\mathbf{x}$. Based on the PSF in (5), the calculation in (3) and (4) can be

further simplified as

$$\gamma_{vu}(\mathbf{x}_0, \mathbf{x}_j) = \frac{1}{\sigma} \sum_{m=1}^{\sigma} \gamma_{vv}(\mathbf{s}_m) \tag{6}$$

$$\gamma_{uu}(\mathbf{x}_i, \mathbf{x}_j) = \frac{1}{\sigma^2} \sum_{m=1}^{\sigma} \sum_{m'=1}^{\sigma} \gamma_{vv}(\mathbf{s}_{mm'}). \tag{7}$$

In (6) and (7), $\sigma = S_u / S_v$ is the pixel size (zoom) ratio between the intermediate and fine pixels, $\mathbf{s}_m$ is the distance between the centroid $\mathbf{x}_0$ of fine pixel v and the centroid of any fine pixel within the intermediate pixel u centered at $\mathbf{x}_j$, and $\mathbf{s}_{mm'}$ is the distance between the centroid of any fine pixel within the intermediate pixel centered at $\mathbf{x}_i$ and the centroid of any fine pixel within the intermediate pixel centered at $\mathbf{x}_j$.

The fine-to-fine semivariogram $\gamma_{vv}(\mathbf{s})$ in (6) and (7) is derived by deconvolution (also called deregularization in geostatistics) of the intermediate (areal) semivariogram, denoted by $\gamma_u(\mathbf{s})$, which is calculated directly from the known intermediate PAN band. Note that $\gamma_u(\mathbf{s})$ is different from $\gamma_{uu}(\mathbf{s})$: the latter is derived by convoluting $\gamma_{vv}(\mathbf{s})$ [see (4)]. The regularized semivariogram $\gamma_u^R(\mathbf{s})$ is calculated as

$$\gamma_u^R(\mathbf{s}) = \gamma_{uu}(\mathbf{s}) - \gamma_{uu}(0). \tag{8}$$

The objective of deconvolution is to estimate the optimal $\gamma_{vv}(\mathbf{s})$, the regularized semivariogram of which approximates $\gamma_u(\mathbf{s})$.

In this paper, an empirical deconvolution approach is developed. In semivariogram modeling, the fitted function is often characterized by three parameters: nugget, sill, and range. To ease the computational burden, the assumption made in [15], [16], and [19] is adopted: there is zero nugget effect in the fine-to-fine semivariogram. The sill and range are determined by referring to the known $\gamma_u(\mathbf{s})$. First, a candidate pool of fine-to-fine semivariograms is generated. For each parameter of $\gamma_{vv}(\mathbf{s})$, two multipliers are empirically defined to generate an interval for selecting the optimal one. The interval for sill selection is set to between 1 and 3 times that of the sill of $\gamma_u(\mathbf{s})$, whereas the interval for range selection is set to between 0.5 and 2.5 times that of the range of $\gamma_v(\mathbf{s})$. The step is 0.1. Second, each semivariogram characterized by the two parameters is convolved to the regularized semivariogram according to (8). Finally, the optimal fine-to-fine semivariogram is determined as the one with the parameter combination leading to the smallest difference between $\gamma_u^R(\mathbf{s})$ and the known $\gamma_u(\mathbf{s})$.

Note that the deconvolution approach presented above is different from that in [25]. The former selects an optimal parameter combination from the empirically predefined candidate pool by testing and comparison, and the solution space is constrained. The deconvolution approach in [25], however, is iterative and fully automated, which seeks the optimal parameter combination from the unconstrained solution space by setting the initialization and stopping rules.

As seen from the deconvolution and convolution processes and (3), (4), and (8), the size of support and the PSF are taken into account explicitly in ATPK. This is different from conventional kriging-based interpolation that treats each observed areal unit (i.e., intermediate pixel here) as a centroid. Following the procedures introduced here, ATPK can be used

easily for downscaling multiple covariates (such as elevation data and field measurement at a spatial resolution finer than the coarse image) in a more general case. For example, in the case involving T groups of covariates with different spatial resolutions, each type of covariate can be downscaled to the target fine spatial resolution according to (1).

C. ATPRK-Based Image Fusion

After the covariates (e.g., PAN) are downscaled to the fine spatial resolution, they are used to model the overall trend of the target variables $\hat{Z}_v^l(\mathbf{x})$ via regression, followed by the postresidual downscaling step with ATPK in ATPRK. Suppose $\hat{Z}_{v1}^l(\mathbf{x})$ and $\hat{Z}_{v2}^l(\mathbf{x})$ are the predictions of the regression and ATPK-derived residuals for coarse band l. The ATPRK prediction is

$$\hat{Z}_v^l(\mathbf{x}) = \hat{Z}_{v1}^l(\mathbf{x}) + \hat{Z}_{v2}^l(\mathbf{x}). \tag{9}$$

The two steps, i.e., regression modeling and residual downscaling, are introduced in the following.

1) Regression Modeling: This phase takes full advantage of the texture information in the fine PAN band. First, the fine PAN band $\hat{Z}_v$ is upscaled to Z_V to match the spatial resolution of each coarse band. Second, the relationship between Z_V and the observed coarse band, for example, band l, is built by linear regression, i.e.,

$$Z_V^l(\mathbf{x}) = a_l Z_V(\mathbf{x}) + b_l + R(\mathbf{x}) \tag{10}$$

where $R(\mathbf{x})$ is a residual term, and the two coefficients a_l and b_l can be estimated by ordinary least squares [26]. Based on the assumption of scale invariance, the regression model in (10) is then used for regression prediction at a specific location $\mathbf{x}_0$ at fine spatial resolution (i.e., coefficients a_l and b_l do not change with the spatial resolution), by taking fine PAN band $\hat{Z}_v$ as input variables, i.e.,

$$\hat{Z}_{v1}^l(\mathbf{x}) = a_l \hat{Z}_v(\mathbf{x}) + b_l. \tag{11}$$

The auxiliary information from other data (but after the downscaling process in Section II-B) can be also favorably incorporated into regression modeling, which involves multivariate regression.

2) Residual Downscaling: Generally, the regression model in (10) is bias, and there are residuals from the regression phase. The residuals at coarse spatial resolution, denoted by $Z_{V2}^l(\mathbf{x})$, are calculated as

$$Z_{V2}^l(\mathbf{x}) = R(\mathbf{x}) = Z_V^l(\mathbf{x}) - [a_l Z_V(\mathbf{x}) + b_l]. \tag{12}$$

The regression-only approach in (11) fails to fully make use of the spectral information of the observed coarse data, and the prediction will lead to obvious spectral distortion. As a complement to the regression step, ATPK-based residual downscaling is performed as a postprocessing step to preserve the spectral properties of the coarse data. ATPK downscales the coarse residuals $Z_{V2}^l(\mathbf{x})$ to fine residuals $\hat{Z}_{v2}^l(\mathbf{x})$.

According to the theoretical basis of ATPK presented in Section II-B, the fine residual $\hat{Z}_{v2}^l(\mathbf{x}_0)$ is calculated as

$$\hat{Z}_{v2}^l(\mathbf{x}_0) = \sum_{i=1}^{N_2} \beta_i Z_{V2}^l(\mathbf{x}_i), \quad \text{s.t.} \sum_{i=1}^{N_2} \beta_i = 1 \tag{13}$$

where β_i is the weight for the ith coarse pixel surrounding the fine pixel centered at $\mathbf{x}_0$, and N_2 is the number of coarse observations. The weights $\{\beta_1, \ldots, \beta_{N_2}\}$ are obtained in the same way as that illustrated in (2)–(8), which starts from fine-to-fine residual semivariogram estimation by deconvolution.

After the residual downscaling process is completed, the prediction is added back to the regression prediction to achieve the final ATPRK prediction, as shown in (9). ATPRK is conducted for each coarse band in turn to produce a fused multispectral image. The implementation of the proposed ATPRK approach that downscales coarse images to a spatial resolution finer than any of the input images is summarized as follows.

Stage 1. Downscaling intermediate covariates with ATPK.

1) Deconvolution for estimation of the fine-to-fine semivariogram $\gamma_{vv}(\mathbf{s})$.
2) Calculation of $\gamma_{vu}(\mathbf{s})$ and $\gamma_{uu}(\mathbf{s})$ by (3) and (4).
3) Calculation of the kriging weights $\{\lambda_1, \ldots, \lambda_{N_1}\}$ by (2).
4) Calculation of $\hat{Z}_v(\mathbf{x}_0)$ by (1).

Stage 2. ATPRK using downscaled fine covariates.

1) Regression modeling by (11).
2) ATPK-based residual downscaling by (13).
3) Combination of regression predictions and downscaled fine residuals by (9).
4) Steps 1–3 are implemented for each coarse band.

In the proposed geostatistical solution to the downscaling problem in Fig. 1, ATPK has twofold functions. It is not only used for downscaling the intermediate covariates but also used for downscaling the residuals from regression. ATPRK falls within the theoretical framework of ATPK, and the former is a special case of the latter: fine spatial resolution covariates are incorporated into ATPK through regression modeling in ATPRK [see (11)]. More precisely, when both coefficients a_l and b_l in the regression model are 0, the coarse residuals $Z_{V2}^l(\mathbf{x})$ in (12) become the coarse variables $Z_V(\mathbf{x})$ in fact, and correspondingly, ATPRK in this case becomes ATPK.

III. EXPERIMENTS

A. Data Sets and Experimental Setup

Two data sets, including a Landsat ETM+ data set and a MODIS data set, were used to examine the proposed downscaling approach. The Landsat data set was supplied by the Government of Canada through Natural Resources Canada, Earth Sciences Sector, Canada Centre for Remote Sensing. The study area is a 15 km × 15 km area in Alberta in Canada. We used 30-m green, red, and near-infrared bands (i.e., bands 2, 3, and 4) and 15-m PAN band 8 in the experiments. The 30-m bands and the PAN band contain 500 × 500 and 1000 × 1000 pixels, respectively. The false color composite of the Landsat image is shown in Fig. 2(a).
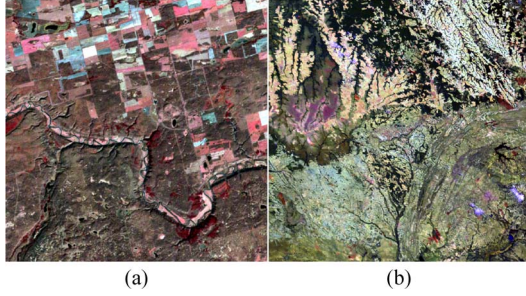
Fig. 2. Data sets used in the experiments. (a) 30-m Landsat data set (500 × 500 pixels; bands 4, 3, and 2 as RGB). (b) 500-m MODIS data set (1000 × 1000 pixels; bands 7, 6, and 4 as RGB).
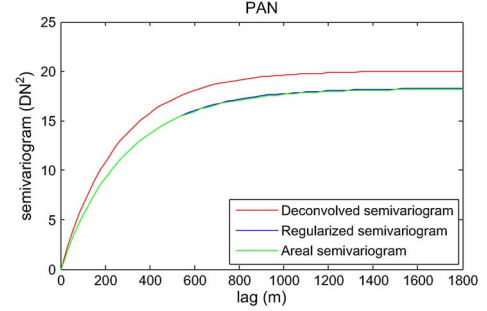

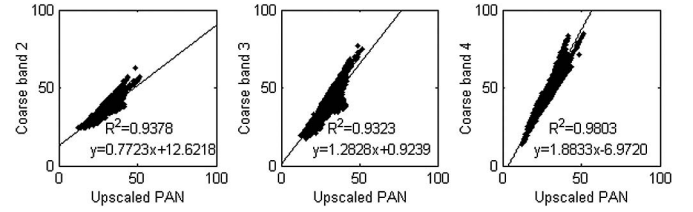Fig. 3. Deconvolution result for the Landsat PAN band.

Fig. 4. Relationship between the Landsat PAN band and the multispectral bands built by linear regression.
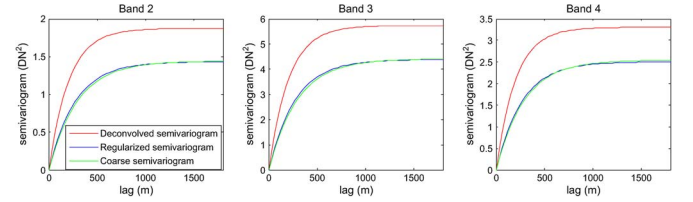

Fig. 5. Deconvolution result for the coarse residuals of the Landsat multispectral bands.

The MODIS data set is a set of MODIS products, including MOD09GQ and MOD09GA. The MOD09GQ product of bands 1 and 2 is provided at 250-m spatial resolution, whereas the MOD09GA product of bands 3–7 is provided at 500-m spatial resolution. The study area is a 500 km × 500 km area of tropical forest in the Brazilian Amazon. Correspondingly, bands 1 and 2 and bands 3–7 have a spatial size of 2000 × 2000 pixels and 1000 × 1000 pixels, respectively. Fig. 2(b) shows the false color composite of the MODIS image. In the experiments, band 5 of the MODIS product MOD09GA was not considered due to the striping artifacts in this band.

Based on the proposed ATPRK approach, the multispectral bands 2–4 in the Landsat image and the bands 3, 4, 6, and 7 in the MODIS image can be downscaled to a spatial resolution finer than 15- and 250-m, for example, 7.5- and 125-m, respectively. In this case, however, no reference at target fine spatial resolution can be used to examine the downscaling results objectively. For quantitative assessment, we upscaled the 30-m Landsat and 500-m MODIS multispectral bands by a factor to synthesize coarse images. Taking the Landsat data set as an example for illustration, the 30-m bands 2–4 and the 15-m PAN band were simultaneously upscaled with a factor of 4 to create 120-m multispectral bands and a 60-m PAN band. The objective of downscaling in the experiments is then to restore the 30-m fine Landsat image, taking the 120-m multispectral bands as observed coarse data and the 60-m intermediate PAN as the covariate. This is the same case for the MODIS data set, which was also upscaled to synthesize 2000-m coarse and 1000-m intermediate images with a factor of 4, and the 500-m fine MODIS image needs to be predicted. The advantage of using synthetic images is that the reference data (i.e., 30-m Landsat and 500-m MODIS images) are known perfectly and can be used objectively to assess the quality of the downscaled products.

Four downscaling approaches, including wavelets [7], HPF [3], KED [17], and DSCK [19], were used as benchmark algorithms to provide a systematic comparison and illustration of the benefits of the new approach. All methods aim to downscale the observed coarse data to the target fine resolution (i.e., 30-m Landsat and 500-m MODIS images). For fair comparison, the four two-stage pansharpening approaches, namely, wavelets, HPF, KED, and ATPRK, used the same ATPK-downscaled fine PAN band (as illustrated in Section II-B) as input for the second stage. DSCK is a one-stage approach, and it directly used intermediate PAN as input [19].

The downscaling results were compared both visually and quantitatively. We used six indices for quantitative evaluation, including the root-mean-square error (RMSE), CC, universal image quality index (UIQI) [27], relative global-dimensional synthesis error (ERGAS) [28], spectral angle mapper (SAM), and spectral information divergence (SID) [29]. The results of the Landsat and MODIS data sets are illustrated in the following two separate sections (see Section III-B and C).

B. Experiment on the Landsat Data Set

1) Implementation: In the first stage, the 60-m intermediate PAN band was downscaled to the 30-m fine PAN band with ATPK. It started from estimation of the 30-m semivariogram for the PAN band, based on the deconvolution approach presented in Section II-A. Fig. 3 shows the deconvolution result for the PAN band (with exponential models for the fitting process). As can be observed from the figure, the regularized and areal semivariograms (both at 60-m) coincide with each other, suggesting the effectiveness of the deconvolution approach.

In the second stage, ATPRK was performed, using the 30-m PAN band produced from the first stage as a fine covariate. Fig. 4 shows the regression models built for the Landsat multispectral bands. Due to the difference in wavelengths, the regression models for the three 120-m bands are noticeably different. Nevertheless, the coefficients of determination (R^2) of all three bands are over 0.93, indicating a high similarity between the coarse bands and the upscaled PAN band. The large association reveals the rationality of the regression process in ATPRK. The regression models in Fig. 4 were used to obtain the 30-m regression predictions, as illustrated in (11). According to (12),
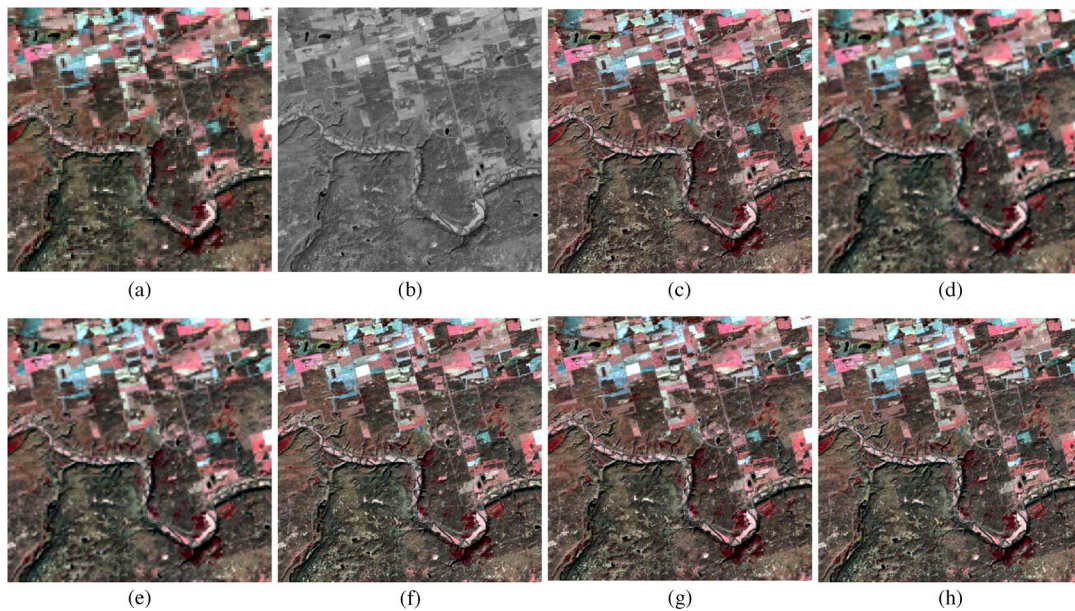
Fig. 6. Downscaling results for the Landsat image. (a) 120-m coarse image. (b) 60-m PAN band. (c) 30-m reference image. (d) Wavelets. (e) HPF. (f) KED. (g) DSCK. (h) ATPRK.

three 120-m coarse residual bands were obtained and then downscaled to 30-m residuals [see (13)]. The corresponding deconvolution results are displayed in Fig. 5, in which the regularized coarse semivariogram coincides with the target coarse semivariogram. Finally, the 30-m regression predictions and residuals were combined to achieve the ATPRK results.

2) Comparison With Other Downscaling Methods: Fig. 6 exhibits the downscaling results of the five methods. For clearer visual comparison between the results, the results of two 200×200 subareas are zoomed in Fig. 7. As shown in the figures, downscaled images are visually clearer than the 120-m coarse image. Wavelets and HPF produced oversmooth results and failed to restore the texture of heterogeneous pixels. The three geostatistical approaches (KED, DSCK, and ATPRK) obviously outperform wavelets and HPF. KED, DSCK, and ATPRK can satisfactorily delineate the boundaries for the homogeneous landscape and reproduce the heterogeneous variation. Note that mosaic pixels exist in several places in the KED result, such as the "white" pixels in Fig. 7(f2). The advantages of the three geostatistical approaches can be also demonstrated by the scatterplots in Fig. 8.

The quantitative assessment for the five methods is listed in Table I. For RMSE, CC, and UIQI, the values of all three bands and their means are listed. Checking the values, the wavelets method has the weakest performance among the five methods. Although HPF is superior to wavelets, the performance is weaker than KED, DSCK, and ATPRK. Moreover, compared with KED and DSCK, ATPRK produced greater CC and UIQI (for all bands) and smaller RMSE (for all bands), ERGAS, SAM, and SID. The quantitative assessment reveals that ATPRK produced the fused image with greater quality than the other four methods.

3) Comparison Between the 60- and 30-m ATPRK-Derived Images: In the proposed ATPRK-based approach, the spatial resolution of the observed coarse Landsat image (i.e., 120-m) was increased to 30 m, which is finer than that of the available

Fig. 7. Downscaling results of two subareas in Fig. 6. (a1) and (a2) 120-m coarse image. (b1) and (b2) 60-m PAN band. (c1) and (c2) 30-m reference image. (d1) and (d2) Wavelets. (e1) and (e2) HPF. (f1) and (f2) KED. (g1) and (g2) DSCK. (h1) and (h2) ATPRK.

PAN band. To illustrate the benefit of the proposed approach, we ran the original ATPRK [18] that used the 60-m PAN band as the covariate directly and produced a 60-m fused image. The 30- and 60-m ATPRK-derived images are shown in Fig. 9 for

Fig. 8. Scatterplots of predicted against actual pixel values (30 m).

TABLE I
QUANTITATIVE ASSESSMENT OF THE FIVE DOWNSCALING METHODS
FOR THE ENTIRE LANDSAT IMAGE (B2, B3, B4, AND M
DENOTE BAND 2, BAND 3, BAND 4, AND MEAN)

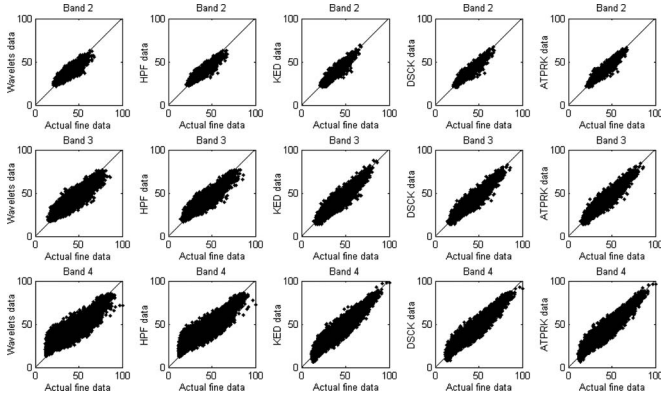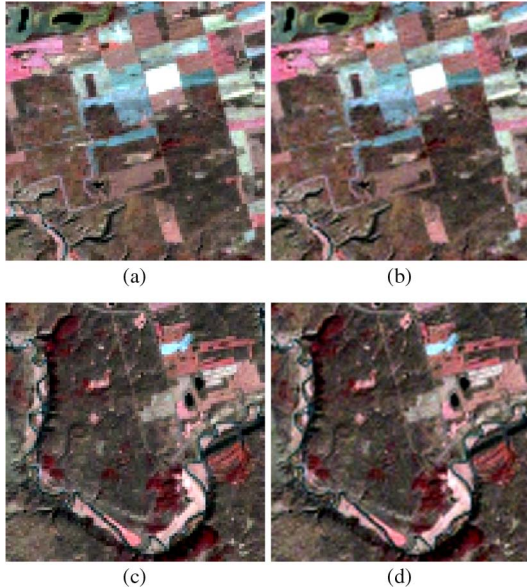|		Ideal	Wavelets	HPF	KED	DSCK	ATPRK
RMSE	B2	0	1.7445	1.4578	1.3900	1.4874	**1.3228**
	B3	0	2.8814	2.5456	2.2168	2.2216	**2.0826**
	B4	0	3.9393	3.5216	2.5303	2.6223	**2.4592**
	M	0	2.8551	2.5084	2.0457	2.1104	**1.9549**
CC	B2	1	0.9047	0.9348	0.9405	0.9396	**0.9463**
	B3	1	0.9082	0.9296	0.9462	0.9486	**0.9526**
	B4	1	0.9118	0.9306	0.9640	0.9627	**0.9660**
	M	1	0.9082	0.9317	0.9502	0.9503	**0.9549**
UIQI	B2	1	0.8974	0.9300	0.9395	0.9384	**0.9455**
	B3	1	0.8980	0.9218	0.9455	0.9473	**0.9518**
	B4	1	0.9012	0.9223	0.9634	0.9618	**0.9655**
	M	1	0.8988	0.9247	0.9495	0.9492	**0.9543**
ERGAS		0	1.9410	1.7105	1.3924	1.4317	**1.3285**
SAM(°)		0	0.0376	0.0369	0.0340	0.0324	**0.0305**
SID		0	0.7031	0.5497	0.3527	0.3736	**0.3238**

Fig. 9. Downscaling results of ATPRK for the Landsat image at 60- and 30-m spatial resolution. (a) and (c) 60-m results. (b) and (d) 30-m results.

visual comparison. It is clear that the 30-m results are smoother, with more elongated features and small patches being better restored. The 30-m fused image is obviously closer to the

TABLE II
QUANTITATIVE ASSESSMENT OF THE 60- AND 30-m ATPRK RESULTS
FOR THE ENTIRE LANDSAT IMAGE (B2, B3, B4, AND M
DENOTE BAND 2, BAND 3, BAND 4, AND MEAN)

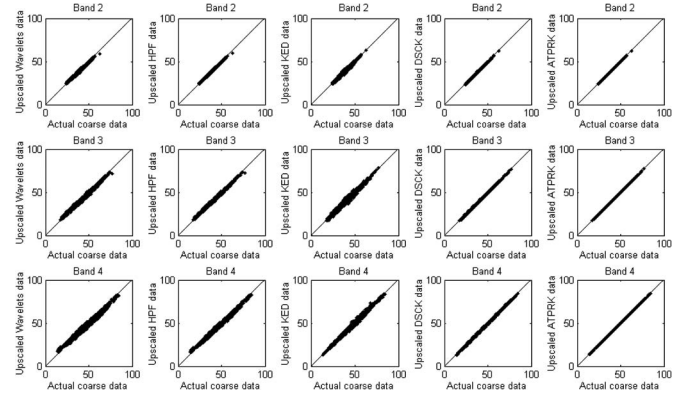|		Ideal	60 m	30 m
RMSE	B2	0	1.4761	**1.3228**
	B3	0	2.3869	**2.0826**
	B4	0	2.9999	**2.4592**
	M	0	2.2877	**1.9549**
CC	B2	1	0.9326	**0.9463**
	B3	1	0.9372	**0.9526**
	B4	1	0.9489	**0.9660**
	M	1	0.9396	**0.9549**
UIQI	B2	1	0.9311	**0.9455**
	B3	1	0.9356	**0.9518**
	B4	1	0.9478	**0.9655**
	M	1	0.9382	**0.9543**
ERGAS		0	1.5541	**1.3285**
SAM(°)		0	0.0324	**0.0305**
SID		0	0.4440	**0.3238**

Fig. 10. Scatterplots of predicted against actual coarse pixel values (120 m).

TABLE III
EVALUATION (IN TERMS OF CC) OF THE ABILITY TO PRESERVE THE
SPECTRAL PROPERTIES OF THE ORIGINAL COARSE LANDSAT IMAGE
(B2, B3, B4, AND M DENOTE BAND 2, BAND 3, BAND 4, AND MEAN)

	Ideal	Wavelets	HPF	KED	DSCK	ATPRK
B2	1	0.9951	0.9981	0.9936	0.9965	**1**
B3	1	0.9946	0.9975	0.9936	0.9985	**1**
B4	1	0.9943	0.9969	0.9979	0.9991	**1**
M	1	0.9947	0.9975	0.9950	0.9980	**1**

reference image [see Fig. 7(c1) and (c2)]. The quantitative comparison from Table II also reveals that the quality of the 30-m fused image is greater than that of the 60-m image. For example, in the image produced with the proposed downscaling scheme, the CC and the UIQI (both mean) are increased by 0.0153 and 0.0161, respectively; and ERGAS and SID are decreased by 0.2256 and 0.1202, respectively.

4) Coherence Characteristic: The coherence characteristic is an important criterion for evaluation of the quality of down-scaled images. This means the ability to conserve spectral properties of the original coarse data. Fig. 10 shows the scatterplots between the upscaled and actual coarse data. Table III lists the corresponding CCs in Fig. 10. Both visual and quantitative statistics indicate that the wavelets approach has the smallest CC overall and that DSCK is superior to HPF and KED (in terms of the coherence characteristic). Furthermore, ATPRK
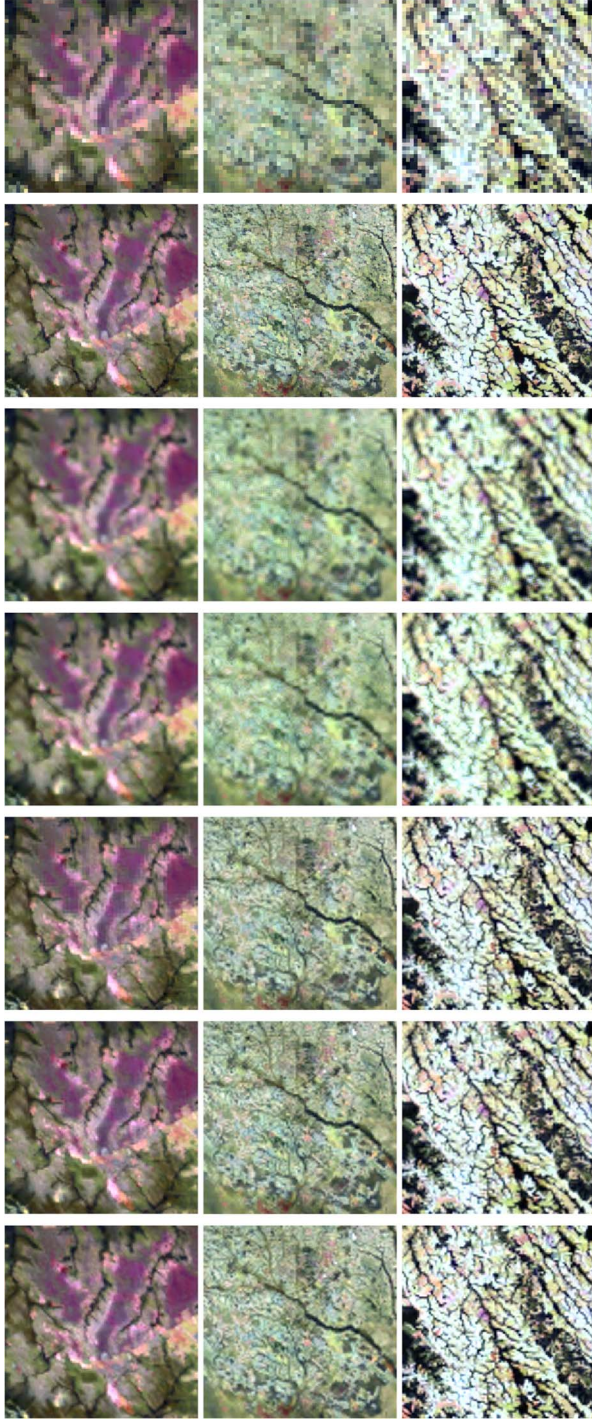
Fig. 11. Downscaling results of three subareas for the MODIS image. (First row) 2000-m coarse image. (Second row) 500-m reference image. (Third row) Wavelets. (Fourth row) HPF. (Fifth row) KED. (Sixth row) DSCK. (Seventh row) ATPRK.

can perfectly preserve the spectral properties of observed coarse data.

C. Experiment on the MODIS Data Set

This section illustrates the performances of downscaling for the MODIS data set. To provide a clear visual assessment, the results of three 200 × 200 subareas are shown in Fig. 11. Focusing on the fused images, the wavelets and HPF results are

TABLE IV
QUANTITATIVE ASSESSMENT OF THE FIVE DOWNSCALING METHODS FOR THE ENTIRE MODIS IMAGE (B3, B4, B6, B7, AND M DENOTE BAND 3, BAND 4, BAND 6, BAND 7, AND MEAN)

		Ideal	Wavelets	HPF	KED	DSCK	ATPRK
RMSE	B3	0	0.0081	0.0060	**0.0048**	**0.0048**	0.0049
	B4	0	0.0095	0.0071	0.0063	**0.0061**	0.0062
	B6	0	0.0398	0.0366	0.0291	0.0280	**0.0276**
	B7	0	0.0371	0.0340	0.0269	0.0261	**0.0258**
	M	0	0.0236	0.0209	0.0168	0.0162	**0.0161**
CC	B3	1	0.9132	0.9535	0.9691	**0.9702**	0.9685
	B4	1	0.9218	0.9576	0.9664	**0.9684**	0.9679
	B6	1	0.9070	0.9222	0.9505	0.9543	**0.9557**
	B7	1	0.9035	0.9199	0.9493	0.9524	**0.9537**
	M	1	0.9114	0.9383	0.9588	0.9614	**0.9615**
UIQI	B3	1	0.9131	0.9535	0.9690	**0.9701**	0.9685
	B4	1	0.9199	0.9568	0.9661	**0.9680**	0.9678
	B6	1	0.8950	0.9126	0.9497	0.9529	**0.9546**
	B7	1	0.8900	0.9092	0.9485	0.9509	**0.9525**
	M	1	0.9045	0.9330	0.9583	0.9605	**0.9609**
ERGAS		0	3.6976	3.1334	2.5283	2.4540	**2.4529**
SAM(°)		0	0.0560	0.0530	0.0438	0.0410	**0.0409**
SID		0	0.0152	0.0121	0.0076	0.0072	**0.0070**

TABLE V
COMPUTATIONAL COSTS OF THE DOWNSCALING METHODS

	Wavelets	HPF	KED	DSCK	ATPRK
Landsat	8.7s	9.0s	136.6s	68.2s	51.3s
MODIS	27.5s	26.8s	597.9s	157.1s	148.8s

ambiguous (particularly in the second subarea), and boundaries cannot be observed clearly (e.g., in the first and third subareas). KED, DSCK, and ATPRK reproduced more heterogeneous variation and delineated clearer boundaries, and their results are closer to the 500-m reference image. Table IV provides a quantitative assessment of the five downscaling methods. Similarly to the Landsat results, the three geostatistical approaches are obviously superior to wavelets and HPF. DSCK and ATPRK have very similar performances (for all four bands), both of which are more accurate than KED in this experiment.

D. Computational Cost

The computational costs of the five downscaling methods are summarized in Table V. All tests were carried out on an Intel Core i7 processor at 3.40 GHz with the MATLAB 7.1 version. Due to the difference in spatial size and number of coarse bands of the Landsat and MODIS data sets, the computing times for the two data sets are different for each method. The wavelets, HPF, and KED methods required downscaled PAN image. Thus, the time spent in ATPK-based PAN downscaling was included in these methods. The wavelets and HPF methods generally have the same computational efficiency, which is greater than the three geostatistical methods. KED takes much more time than DSCK and ATPRK, and this is more obvious for the MODIS image. This is because KED calculates the kriging weights locally for each fine pixel and its computational cost increases linearly with the number of fine pixels to be predicted. Both DSCK and ATPRK calculate the kriging weights only once for the entire image and, thus, release the computational burden in KED. Furthermore, ATPRK takes less time than DSCK, as DSCK considers the extra cross-semivariogram

modeling (e.g., deconvolution and convolution) for each coarse band.

IV. DISCUSSION

A. Contributions

This paper presents a theoretical framework for remote sensing downscaling, which aims to produce fused images with a spatial resolution finer than any of the input variables (even finer than that of the PAN band). The contributions of this paper lie in the theoretical innovation, technological advancement, and application value.

Theoretically, a new geostatistical solution based on ATPRK is proposed for the downscaling problem defined in Fig. 1, which treats the observed coarse data as primary variables and the intermediate PAN band as a type of covariate. ATPRK is a new image fusion approach based on a new conceptualization that is originally defined in geostatistics. It serves as a new bridge between geostatistics and remote sensing [30]. It will motivate other further exploration of this new geostatistical solution to image fusion in future research.

Technologically, in the first stage, the intermediate covariates (i.e., PAN band in this paper) are proposed to be downscaled to the target fine spatial resolution with general ATPK. ATPK is performed with an empirical, but effective, deconvolution approach (see, for example, Fig. 3) as an initial point. In the second stage, the fine covariates are used in ATPRK, which first constructs the relationship between the primary variables and available covariates by regression modeling and then downscales the coarse residuals from the regression process with ATPK. The downscaled residuals are finally added back to the regression predictions to achieve image fusion. The new downscaling approach accounts for size of support, spatial correlation, and the PSF of the sensor and maintains a perfect coherence characteristic, as demonstrated by the experimental results in Section III-B4 (the theoretical proof runs parallel to the proof presented in [18]). Moreover, the new downscaling approach is user friendly and can be extended readily by the use of ancillary information provided by other data. Access to additional covariates would lead to further enhancement of the current version of ATPRK.

The proposed downscaling approach has great potential for finer spatial resolution LCLU monitoring at the global scale than the currently available remote sensing images. The MODIS and Landsat images are common sources for global LCLU monitoring (e.g., MODIS data for monitoring deforestation over the Amazon rainforest and Landsat data for monitoring urbanization over highly developed cities) due to their free availability, wide swath, and regular revisit capability [31], [32]. The new ATPRK-based geostatistical solution was examined for both MODIS and Landsat images in the experimental studies. It was demonstrated that the proposed approach can produce fused images at a spatial resolution finer than the PAN band with satisfactory performances. Moreover, ATPRK is more accurate than the other benchmark methods, and it can precisely conserve the spectral properties of the observed coarse data. The encouraging results for the MODIS and Landsat images produced here will promote the adoption of the new downscaling approach in practical and operational applications. For example, with the new approach, MODIS and

TABLE VI
COMPARISON BETWEEN THREE GEOSTATISTICAL SOLUTIONS

	One-stage	Cross-semivariogram modelling	Size of kriging matrices	Computational cost
DSCK	Yes	Yes	DSCK>	KED>
KED	No	No	KED>	DSCK>
ATPRK	No	No	ATPRK	ATPRK

Landsat images can be downscaled to a spatial resolution such as 125- and 7.5-m, respectively. Based on the fused products, more detailed LCLU information can be obtained for global monitoring.

B. Intercomparison Between KED-, DSCK- and ATPRK-Based Geostatistical Solutions to Downscaling

DSCK is a one-stage downscaling approach that considers the primary variable (observed coarse band) and secondary variable (ancillary PAN band) simultaneously, by including both autosemivariograms and cross-semivariogram(s) in the kriging matrices [19]. However, both the autosemivariogram and cross-semivariogram need to be computed for each coarse band, which involves complex deconvolution and convolution calculation processes. For example, for the three-band Landsat and four-band MODIS data sets in the experiments, six and eight deconvolved semivariograms were computed, respectively. This would sometimes require manual intervention, particularly for the cross-semivariogram modeling. Essentially, in DSCK, the cross-semivariogram accounts for the cross correlation between the observed coarse band and the intermediate PAN band. ATPRK simplifies the process noticeably by using the simple regression models in (10) and (11) instead. ATPRK requires only autosemivariogram modeling, and all calculations occur in each coarse band separately. Thus, the size of the kriging matrices in ATPRK is much smaller than that in DSCK, which is more obvious when the number of covariates is large. In addition, the increased size of DSCK kriging matrices might lead to an unstable matrix and further decreased accuracy in downscaling, as illustrated in the Landsat results in Table I. Although ATPRK is not a one-stage process as covariates need to be downscaled to the fine spatial resolution in advance, it is much easier to automate and more user friendly.

Similarly to ATPRK, KED in this paper requires downscaled covariates and is not a one-stage approach. As an alternative to DSCK, KED does not require the cross-semivariogram [17]. However, KED also extends the kriging matrices by including the covariates and would result in unstable matrix [33], as occurred in DSCK. Moreover, KED calculates the kriging weights locally for each fine pixel, which greatly increases the computational cost, particularly for large areas. ATPRK, however, separates trend estimation (i.e., regression modeling) from residual downscaling. As a result, the ATPRK kriging weights are calculated only once, and thus, ATPRK is a fast image downscaling approach free of the risk of instability in the kriging weights calculation. Table VI summarizes the differences between the three geostatistical approaches.

C. Future Research

In the experiments, the proposed approach was demonstrated to be effective in downscaling the Landsat and MODIS data

sets. The encouraging results for the two types of images with different spatial resolutions will motivate its application to more types of remote sensing images, including very high resolution remote sensing products (such as IKONOS, QuickBird, and WorldView) [34], [35] and hyperspectral images [12], [36], [37]. This has been a lively topic in the remote sensing community in recent years.

In ATPRK, ATPK-based residual downscaling satisfactorily compensates for the residuals from regression to the fine pixels. In the regression part, based on the hypothesis of scale invariance, the regression model fitted at coarse spatial resolution in (10) is used for regression prediction at fine spatial resolution, as shown in (11). This hypothesis may work better for homogeneous pixels. For heterogeneous pixels, where the spatial pattern changes sharply, the regression model in (10) might be insufficient for characterizing the relationship at fine spatial resolution. As observed from Fig. 4, the linear regression may sometimes not be sufficient to model the relationship between the covariate and the observed coarse data. It would be worthwhile to develop new regression models (e.g., spatially adaptive regression model that can separate homogeneous and heterogeneous pixels) with more powerful modeling ability for further possible enhancement of ATPRK.

The proposed approach allows the use of multiple covariates with different intermediate spatial resolutions. Specifically, the multiple covariates can be downscaled separately to the target fine spatial resolution according to (1). The relationship between the multiple fine covariates and observed coarse data can be built via multivariate regression, a process similar to that in (10) and (11). Theoretically, the proposed approach can downscale the coarse multispectral bands to a spatial resolution (denoted by A m) finer than that of the covariates with the finest spatial resolution (denoted by B m). However, the zoom ratio B/A should not be too large, and generally, a zoom factor between 2 and 4 is suggested. This is because downscaling is essentially an ill-posed problem, and as the zoom ratio increases, the number of subpixels to be predicted within each coarse pixel increases quadratically, which increases the uncertainty in downscaling. The ease of incorporating multiple covariates provides an interesting avenue for future research, where more relevant information on the studied areas is encouraged to be sought.

V. Conclusion

In this paper, an ATPRK-based geostatistical solution has been proposed to downscale remote sensing images to a spatial resolution finer than that of any of the input images. The PAN band is considered as an intermediate covariate, and its spatial resolution is increased to the target fine spatial resolution with general ATPK. The ATPK-derived fine PAN band is used by ATPRK to sharpen the coarse bands, which consists of regression modeling between the fine PAN and observed coarse bands and ATPK-based residual downscaling. The proposed approach was tested using a Landsat data set and a MODIS data set. The conclusions from the experiments are summarized as follows: 1) Compared with the original ATPRK approach that produces sharpened images with the same spatial resolution as the PAN band [18], the new ATPRK-based geostatistical solution can produce sharpened images at a *finer* spatial resolution with greater quality in terms of the six indices (i.e., RMSE, CC, UIQI, ERGAS, SAM, and SID). 2) Compared with wavelets, HPF, KED, and DSCK, ATPRK is able to produce more accurate fused images in terms of the six indices. 3) ATPRK can precisely conserve the spectral content of the original coarse images.
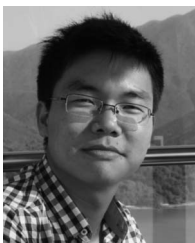
References

[1] M. C. Hansen, Y. E. Shimabukuro, P. Potapov, and K. Pittman, "Comparing annual MODIS and PRODES forest cover change data for advancing monitoring of Brazilian forest cover," *Remote Sens. Environ.*, vol. 112, no. 10, pp. 3784–3793, Oct. 2008.

[2] M. Castrence, D. H. Nong, C. C. Tran, L. Young, and J. Fox, "Mapping urban transitions using multi-temporal Landsat and DMSP-OLS night-time lights imagery of the red river delta in Vietnam," *Land*, vol. 3, no. 1, pp. 148–166, Feb. 2014.

[3] P. S. Chavez, Jr., S. C. Sides, and J. A. Anderson, "Comparison of three different methods to merge multiresolution and multispectral data: Landsat TM and SPOT panchromatic," *Photogramm. Eng. Remote Sens.*, vol. 57, no. 3, pp. 295–303, Mar. 1991.

[4] A. R. Gillespie, A. B. Kahle, and R. E. Walker, "Color enhancement of highly correlated images—II. Channel ratio and 'chromaticity' transformation techniques," *Remote Sens. Environ.*, vol. 22, no. 3, pp. 343–365, Aug. 1987.

[5] V. K. Shettigara, "A generalized component substitution technique for spatial enhancement of multispectral images using a higher resolution data set," *Photogramm. Eng. Remote Sens.*, vol. 58, no. 5, pp. 561–567, May 1992.

[6] J. Nunez *et al.*, "Multiresolution-based image fusion with additive wavelet decomposition," *IEEE Trans. Geosci. Remote Sens.*, vol. 37, no. 3, pp. 1204–1211, May 1999.

[7] B. Aiazzi, L. Alparone, S. Baronti, and A. Garzelli, "Context-driven fusion of high spatial and spectral resolution images based on oversampled multi-resolution analysis," *IEEE Trans. Geosci. Remote Sens.*, vol. 40, no. 10, pp. 2300–2312, Oct. 2002.

[8] Q. Wei, J. Bioucas-Dias, N. Dobigeon, and J. Tourneret, "Hyperspectral and multispectral image fusion based on a sparse representation," *IEEE Trans. Geosci. Remote Sens.*, vol. 53, no. 7, pp. 3658–3668, Jul. 2015.

[9] Y. Zhang, "Understanding image fusion," *Photogramm. Eng. Remote Sens.*, vol. 70, no. 6, pp. 657–661, Jun. 2004.

[10] C. Pohl and J. L. Van Genderen, "Review article multisensor image fusion in remote sensing: Concepts, methods and applications," *Int. J. Remote Sens.*, vol. 19, no. 5, 823–854, Jan. 1998.

[11] Z. Wang, D. Ziou, C. Armenakis, D. Li, and Q. Li, "A comparative analysis of image fusion methods," *IEEE Trans. Geosci. Remote Sens.*, vol. 43, no. 6, pp. 1391–1402, Jun. 2005.

[12] J. Bioucas-Dias *et al.*, "Hyperspectral remote sensing data analysis and future challenges," *IEEE Geosci. Remote Sens. Mag.*, vol. 1, no. 2, pp. 6–36, Jun. 2013.

[13] G. Vivone *et al.*, "A critical comparison among pansharpening algorithms," *IEEE Trans. Geosci. Remote Sens.*, vol. 53, no. 5, pp. 2565–2586, May 2015.

[14] J. Zhang, "Multi-source remote sensing data fusion: Status and trends," *Int. J. Image Data Fusion*, vol. 1, no. 1, pp. 5–24, Mar. 2010.

[15] E. Pardo-Igúzquiza, M. Chica-Olmo, and P. M. Atkinson, "Downscaling cokriging for image sharpening," *Remote Sens. Environ.*, vol. 102, no. 1/2, pp. 86–98, May 2006.

[16] E. Pardo-Iguzquiza, V. F. Rodríguez-Galiano, M. Chica-Olmo, and P. M. Atkinson, "Image fusion by spatially adaptive filtering using downscaling cokriging," *ISPRS J. Photogramm. Remote Sens.*, vol. 66, no. 3, pp. 337–346, May 2011.

[17] M. H. R. Sales, C. M. Souza, Jr., and P. C. Kyriakidis, "Fusion of MODIS images using kriging with external drift," *IEEE Trans. Geosci. Remote Sens.*, vol. 51, no. 4, pp. 2250–2259, Apr. 2013.

[18] Q. Wang, W. Shi, P. M. Atkinson, and Y. Zhao. Downscaling MODIS images with area-to-point regression kriging. *Remote Sens. Environ.*, vol. 166, pp. 191–204, Sep. 2015.

[19] P. M. Atkinson, E. Pardo-Igúzquiza, and M. Chica-Olmo, "Downscaling cokriging for super-resolution mapping of continua in remotely sensed images," *IEEE Trans. Geosci. Remote Sens.*, vol. 46, no. 2, pp. 573–580, Feb. 2008.

[20] T. Hengl, G. B. M. Heuvelink, and A. Stein, "A generic framework for spatial prediction of soil variables based on regression-kriging," *Geoderma*, vol. 120, no. 1/2, pp. 75–93, May 2004.

[21] T. Hengl, G. B. M. Heuvelink, and D. G. Rossiter, "About regression-kriging: From equations to case studies," *Comput. Geosci.*, vol. 33, no. 10, pp. 1301–1315, Oct. 2007.

[22] P. Kyriakidis and E.-H. Yoo, "Geostatistical prediction and simulation of point values from areal data," *Geograph. Anal.*, vol. 37, no. 2, pp. 124–151, Apr. 2005.

[23] P. C. Kyriakidis, "A geostatistical framework for area-to-point spatial interpolation," *Geograph. Anal.*, vol. 36, no. 3, pp. 259–289, Jul. 2004.

[24] P. M. Atkinson, "Downscaling in remote sensing," *Int. J. Appl. Earth Observ. Geoinf.*, vol. 22, pp. 106–114, Jun. 2013.

[25] P. Goovaerts, "Kriging and semivariogram deconvolution in presence of irregular geographical units," *Math. Geosci.*, vol. 40, no. 1, pp. 101–128, 2008.

[26] P. Kitanidis, "Generalized covariance functions in estimation," *Math. Geol.*, vol. 25, no. 5, pp. 525–540, Jul. 1994.

[27] Z. Wang and A. C. Bovik, "A universal image quality index," *IEEE Signal Process. Lett.*, vol. 9, no. 3, pp. 81–84, Mar. 2002.

[28] T. Ranchin and L. Wald, "Fusion of high spatial and spectral resolution images: The ARSIS concept and its implementation," *Photogramm. Eng. Remote Sens.*, vol. 66, no. 1, pp. 49–61, Jan. 2000.

[29] C. Chang, "Spectral information divergence for hyperspectral image analysis," in *Proc. IEEE Int. Geosci. Remote Sens. Symp.*, 1999, vol. 1, pp. 509–511.

[30] F. D. van der Meer, "Remote-sensing image analysis and geostatistics," *Int. J. Remote Sens.*, vol. 33, no. 18, pp. 5644–5676, Sep. 2012.

[31] Q. Wang, P. M. Atkinson, and W. Shi, "Fast subpixel mapping algorithms for subpixel resolution change detection," *IEEE Trans. Geosci. Remote Sens.*, vol. 53, no. 4, pp. 1692–1706, Apr. 2015.

[32] Q. Wang, W. Shi, P. M. Atkinson, and Z. Li, "Land cover change detection at subpixel resolution with a Hopfield neural network," *IEEE J. Sel. Topics Appl. Earth Observ. Remote Sens.*, vol. 8, no. 3, pp. 1339–1352, Mar. 2015.

[33] P. Goovaerts, *Geostatistics for Natural Resources Evaluation*. London, U.K.: Oxford Univ. Press, 1997.

[34] L. Alparone *et al.*, "Comparison of pansharpening algorithms: Outcome of the 2006 GRS-S data-fusion contest," *IEEE Trans. Geosci. Remote Sens.*, vol. 46, no. 10, pp. 3012–3021, Oct. 2007.

[35] L. Zhang, H. Shen, W. Gong, and H. Zhang, "Adjustable model-based fusion method for multispectral and panchromatic images," *IEEE Trans. Syst., Man, Cybern. B, Cybern.*, vol. 42, no. 6, pp. 1693–1704, Dec. 2012.

[36] G. A. Licciardi *et al.*, "Fusion of hyperspectral and panchromatic images using multiresolution analysis and nonlinear PCA band reduction," *EURASIP J. Adv. Signal Process.*, vol. 2012, no. 1, pp. 207:1–207:17, Sep. 2012.

[37] L. Loncan *et al.*, "Hyperspectral pansharpening: A review," *IEEE Geosci. Remote Sens. Mag.*, vol. 3, no. 3, pp. 27–46, Sep. 2015.

Wenzhong Shi received the Ph.D. degree from Osnabrück University, Vechta, Germany, in 1994.

He is currently a Chair Professor of geographical information science (GIS) and remote sensing and the Head of the Department of Land Surveying and Geo-Informatics, The Hong Kong Polytechnic University, Kowloon, Hong Kong. He is also currently with Wuhan University, Wuhan, China. He has authored or coauthored over 130 Science Citation Index papers and ten books. His current research interests include GIS and remote sensing, uncertainty and spatial data quality control, and image processing for high-resolution satellite images.

Prof. Shi was a recipient of the State Natural Science Award from the State Council of China in 2007 and The Wang Zhizhuo Award from the International Society for Photogrammetry and Remote Sensing in 2012.

Peter M. Atkinson received the B.Sc. degree in geography from The University of Nottingham, Nottingham, U.K., in 1986, the Ph.D. degree from The University of Sheffield (NERC CASE award with Rothamsted Experimental Station), Sheffield, U.K., in 1990, and the MBA degree from the University of Southampton, Southampton, U.K., in 2012.

He is currently the Dean of the Faculty of Science and Technology, Lancaster University, Lancaster, U.K. He has been a Professor of geography with the University Southampton (for the last 21 years; 13 years as Professor), where he is currently Visiting Professor. He is also currently a holder of the Belle van Zuylen Chair in the Faculty of Geosciences with Utrecht University, Utrecht, The Netherlands, and a Visiting Professor with Queen's University Belfast, Belfast, U.K. He has authored or coauthored around 200 peer-reviewed articles in international scientific journals and around 50 refereed book chapters. He has also edited nine journal special issues and eight books. The main focus of his research is in remote sensing, geographical information science, and spatial (and space–time) statistics applied to a range of environmental science and socioeconomic problems.

Dr. Atkinson is an Associate Editor of *Computers and Geosciences* and sits on the editorial boards of several other journals, including *Geographical Analysis*, *Spatial Statistics*, the *International Journal of Applied Earth Observation and Geoinformation*, and *Environmental Informatics*. He sits on various international scientific committees.

Qunming Wang (M'15) received the B.S. degree and M.S. degree from Harbin Engineering University, China, in 2010 and 2012, and the Ph.D. degree from The Hong Kong Polytechnic University, Hong Kong, in 2015. He is now a Senior Research Associate in Lancaster Environment Centre, Lancaster University, U.K.

From June to December 2013, he was a Visiting Ph.D. Student with Geography and Environment, University of Southampton, Southampton, U.K. He has authored or coauthored over 20 peer-reviewed articles in international journals such as *Remote Sensing of Environment*, the IEEE TRANSACTIONS ON GEOSCIENCE AND REMOTE SENSING, and *ISPRS Journal of Photogrammetry and Remote Sensing*. His current research interests focus on remote sensing image analysis and geostatistics.

Dr. Wang serves as a reviewer for over ten international journals. He was awarded the hypercompetitive Hong Kong Ph.D. Fellowship to support his three-year Ph.D. study. He was a recipient of the Excellent Master Dissertation Award and the Excellent Graduates in Heilongjiang Province, China, in 2012.

Eulogio Pardo-Igúzquiza received the Ph.D. degree in geology and statistics from the University of Granada, Granada, Spain, in 1991.

In 1995, he was awarded a two-year postdoctoral grant by the Spanish Ministry of Science and Education. In 1997, he was awarded a two-year Marie Curie fellowship by the European Union to undertake research at the University of Reading, Reading, U.K. In 2000, he moved to Universidad Politécnica de Cataluña, Barcelona, Spain. In July 2003, he was awarded a Ramón y Cajal fellowship to undertake research at the University of Granada. During this time, he paid short visits to Southampton and the Department of Statistics at Leeds. He obtained the post of Lecturer at the University of Granada in 2008. In 2010, he moved to Madrid to take up a position as Research Scientist at the Geological Survey of Spain, Madrid, Spain. He has recently published *Geomatemáticas*, a popular science book on geomathematics.

Dr. Pardo-Igúzquiza is the Editor-in-Chief of *Boletín Geológico y Minero*.